Angle-resolved electron-energy-loss study of Al/Si(111)

P. Akavoor, G. S. Glander,* L. L. Kesmodel,† and Kieron Burke
Department of Physics, Indiana University, Swain West 117, Bloomington, Indiana 47405
(Received 19 March 1993)

We have performed a high-resolution electron-energy-loss study of the Si(111)-($\sqrt{3} \times \sqrt{3}$)$R30°$:Al surface and have measured the dispersions of several surface phonons along the $\overline{\Gamma K}$ direction. We interpret these using two different simple lattice dynamical models, both employing force constants from an *ab initio* electronic-structure calculation of Northrup. The first yields quantitative information at $q = 0$; the second is a semiquantitive estimate of the dispersion. These models have no adjustable parameters. The good agreement with the experiment for most of the observed modes indicates that a single theory can explain both the electronic structure and vibrational modes of this surface and also illustrates both the usefulness and limitations of simple models of lattice dynamics.

I. INTRODUCTION

In the study of a given surface, the electronic structure[1] and vibrational modes[2] are frequently investigated separately, both in calculations and experiments. However, the force constants which determine the lattice dynamics may themselves be determined from the ground-state energies of the electrons when the nucleii are displaced from equilibrium. Thus a complete theory of a surface system can, in principle, account for the ground-state configuration, the electronic structure, and the phonon dispersions.[3–7]

The metal-semiconductor system Si(111)-($\sqrt{3} \times \sqrt{3}$)$R30°$:Al presents an ideal challenge in this respect. The Al adatoms are strongly bound to their neighboring Si atoms, so one can expect several surface phonons to be detectable with energies up to about 100 meV. The frequencies of these phonons and their dispersions provide strict limitations on any theory which includes the lattice dynamics. Moreover, this system has already been investigated with several experimental probes. Low-energy electron diffraction (LEED) analysis indicates that the Al absorbs at the T_4 site,[8] while the unoccupied surface states have been studied using angle-resolved inverse photoemission.[9] Both the ground-state configuration and the positions of the surface states agree well with total energy electronic-structure calculations of Northrup.[10,11] These calculations were extended to include small displacements away from equilibrium,[12] yielding force constants for a $q = 0$ dynamical calculation, producing one phonon at 69 meV and another at 32 meV. The first of these was observed using electron-energy-loss spectroscopy by Kelly *et al.*,[13,14] while the second was seen in a higher resolution study by Glander, Akavoor, and Kesmodel.[15]

In the present work, we report experimental results for the dispersion of several surface phonons along $\overline{\Gamma K}$ for Si(111)-($\sqrt{3} \times \sqrt{3}$)$R30°$:Al. These were found using angle-resolved high-resolution electron-energy-loss spectroscopy (HREELS), in which both dipole and impact scattering were observed. A total of five modes were detected, none of which dispersed strongly. Apart from the two mentioned above, three more, at about 16 meV, 42 meV, and 58 meV, were seen.

To understand the origin and nature of these modes, we solve two distinct lattice dynamical models of this surface. Neither yields a complete description of the dynamics, but together they explain most of the features seen in the experiment. Both include some of the long-wavelength low-frequency features not seen in the earlier work.

In the first of these, we couple the layers of Northrup's $q = 0$ calculation to the Si(111) layers of the bulk below. We restrict their movement to that of rigid planes moving perpendicularly to the surface and coupled by bulk planar force constants.[16] The most significant sources of error in such a model are the exclusion of motions of the bulk lattice which are folded into the $q = 0$ point in the surface unit cell by the surface reconstruction, and of those motions polarized within the surface plane. We find several strong surface resonances in this calculation. At $q = 0$ one expects the scattering to be predominately dipole in origin,[17] and we assume the strongest dipole lies along the Al-Si stretch, where the Si atom is that directly beneath the Al. When the density of states is projected onto this stretch, we find only three remaining strong peaks: at 33 meV, 45 meV, and 69 meV. Thus this simple one-dimensional chain calculation explains three of the five features of the experiment.

In a second calculation, we estimate individual interatomic force constants from planar force constants for the surface layers. This allows us to include dispersion. We also couple these layers to an underlying elastic continuum model.[6] We find that indeed there is little dispersion, and we can also follow the Rayleigh wave throughout the zone. The 16-meV mode of the experiment is simply the folded-back branch of the Rayleigh wave while the acoustic branch is not seen in the experiment as it is washed out by the large elastic peak.

Neither of these models is intended as a full lattice dynamical calculation, but only as a preliminary guide to help interpret the experimental results. In particular, the

observed 60-meV mode does not occur in either of them. This is probably a Lucas mode, as has been seen on other Si(111) surfaces.[18,19] It would not appear in our first model if it were either a folded-in zone-boundary mode or a saggital-plane polarized transverse mode. On the other hand, the good agreement with the other observed modes suggests that Northrup's electronic-structure calculations yield a consistent picture of the surface geometry, electronic spectrum, and vibrational spectrum.

Section II is an account of how the experiment was performed, including how peak positions were deduced from the data. Section III is a description of the two different lattice dynamical models we use. In Sec. IV we make a detailed comparison between these models and the experiment. We give our conclusions in Sec. V.

II. EXPERIMENT

The ultrahigh vacuum chamber used in this study was composed of two parts. The upper portion of the chamber was equipped with a rotatable flange which supported the sample manipulator built by Vacuum Generators Ltd. (model HPLT305). The manipulator employed a dual bellows system. One of the bellows allowed the X and Y (lateral) movements and the other, the Z (vertical) movement. Rotational motion was achieved by precision rotary drives (model RD2-S) fitted on the manipulator. One could rotate the sample about the Z axis and about an axis perpendicular to the Z axis. The upper chamber also housed equipment for surface analyses. This equipment consisted of an Inficon mass spectrometer for residual gas analyses, a Varian sputtering gun, and a Varian retarding field analyzer for LEED and Auger electron spectroscopy. The lower portion of the chamber housed the HREEL spectrometer and was connected to a Perkin-Elmer ion pump.

A schematic diagram of the HREEL spectrometer is given in Fig. 1. The spectrometer had a dual monochromator, a single stage 127° cylindrical deflection analyzer, and a channeltron detector. A dual monochromator was chosen to avoid problems of space charging which may occur at high feed currents in stage 1 of the monochromator and to provide a low spectral background free of "ghost peaks." The principle and operation of the spectrometer have been thoroughly studied in the literature.[20] The design was similar to that described elsewhere.[21] However, in the present system the detector angle α could be varied from 13° to 68°. This facilitated angle-resolved measurements.

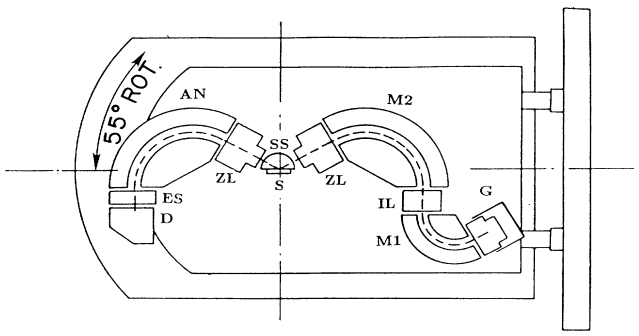

FIG. 1. Schematic of the apparatus: electron gun (G), monochromator stage 1 (M1), mononchromator stage 2 (M2), zoom lenses (ZL), sample (S), sample shield (SS), intermediate lenses (IL), analyzer (AN), and detector (D) are shown.

The samples, roughly 0.5 cm × 0.5 cm in size, were single crystals cut from a commercial wafer of Si(111)(8–12 Ω cm, P doped). The samples were mounted on Mo stubs that were transferred in and out of the chamber using a load lock and a wobble stick.

To heat the sample, we used a modified version of the standard resistive heater built into the Vacuum Generators sample manipulator. The heater consisted of a coil of 8-mil-diam tungsten wire encased in alumina tubing inside the sample manipulator. To improve the heating of the sample, we machined holes in the front plate of the sample manipulator and in the Mo stub so that the back side of the Si sample was heated by direct radiation from the heater coil. This arrangement allowed us to reach maximum temperatures of the order of 900 °C. Still higher temperatures could be achieved, and temperatures of the order of 900 °C could be reached more quickly by adding the capability to position the sample in front of an auxiliary tungsten heater that radiantly heated the front of the sample. Care was taken to install radiation shields behind the heater coil to minimize radiation losses.

Fresh Si samples were annealed *in vacuo* at 900 °C for an hour and subsequently cooled at a rate of about 1 °C/s. This annealing was done slowly so that the pressure in the chamber would not rise above 1.0×10^{-9} Torr. After such a heat treatment, no contaminants were detected in the Auger spectra of the samples. LEED consistently showed excellent Si-(7×7) patterns. Aluminum was deposited onto the Si samples from a braided W filament wrapped with 99.999%-pure Al wire. The amount of Al deposited was monitored with a quartz-crystal microbalance, which was placed at about $\frac{1}{6}$ the filament-to-sample separation so that it was sensitive to submonolayer coverages on the sample. Before we actually deposited any Al on the substrate, we slowly stepped up the current through the braided tungsten filament and carefully outgassed it. Assignment of different coverages was primarily done using the LEED pattern. We relied on the microbalance as a secondary scale for the coverage, using it mainly to quantify the relative amounts of Al used in various experiments and to determine the best operating conditions for the Al source each time the filament was replaced. There was good agreement between the calculated and observed frequency changes of the quartz crystal for the various coverages.

As reported earlier,[15] we were able to obtain different ordered structures depending on the quantity of Al deposited. Deposition of $\frac{1}{3}$ of a monolayer (ML) produced a $\sqrt{3}\times\sqrt{3}$ LEED pattern; $\frac{3}{7}$ of a ML produced $\sqrt{7}\times\sqrt{7}$ pattern; and 1 ML produced (7×7)-Al pattern. The most reliable procedure to produce the $\sqrt{3}\times\sqrt{3}$ surface was to deposit about $\frac{1}{3}$ ML of Al, heat the sample to 800 °C, and

cool immediately. Similarly, the $\sqrt{7}\times\sqrt{7}$ and the (7×7)-Al surfaces were produced by depositing the appropriate amounts of Al and by flash annealing to 800 °C. During deposition of Al, the substrate temperature was typically in the range of 200 °C–300 °C. It may be noted that depositing intermediate amounts of Al produced mixed structures. Heating to 900 °C for about 5 min removed all Al and cooling slowly restored the familiar Si-(7×7) LEED pattern.

One of the technical problems was that any time Al was exposed to oxygen, alumina was formed. Any alumina near the sample charged up and this caused degradation of the resolution. To circumvent this problem, we had to remove all of the native oxide off the sample stub before depositing any Al. Similarly, all of the Al had to be removed before a sample stub was taken out into air for sample change. This was done by sputtering and annealing after which no significant amount of oxide or Al was detected in the Auger spectra of the stub or the sample. Exposing the stub to atmosphere for 10–15 min during a sample change did produce a thin layer of oxide. But this thin layer was easily removed by heating to 900 °C for about 1 h. Another technical problem involved the presence of a small amount of hydrocarbon contamination in the chamber. Although no contaminants were detected in the Auger spectra initially, after three or four days a small C peak appeared. At this point, we discarded the sample.

For the $\sqrt{3}\times\sqrt{3}$ surface, we acquired the loss spectra for nonzero q values by rotating the energy analyzer through the desired angle. During off-specular measurements, we periodically rotated the analyzer back to the specular direction and repeated the measurement. This procedure helped us determine whether a certain surface had degraded over time. We also checked the LEED pattern to make sure that the surface still showed a good $\sqrt{3}\times\sqrt{3}$ LEED pattern. Fuzzy third-order LEED spots and an increase in diffuse scattering usually indicated a degraded surface. Duration of a well-prepared surface was typically 5–6 h.

Each spectrum was fitted to a series of Gaussian curves superimposed on a linear background. Typical spectra are shown in Fig. 2. The spectrum in Fig. 2(a) contains specular ($q = 0$) data. The incident beam energy was 3 eV and the full width at half maximum (FWHM) for the elastic peak was 6.6 meV. We do not believe that the weak feature around 76 meV is due to the $\sqrt{3}\times\sqrt{3}$ structure for the following reason. HREEL spectra taken at various times as the surface degraded showed that most of the loss peaks decreased in intensity while the feature around 76 meV grew in intensity to eventually dominate the region of the spectrum.[15] The spectrum in Fig. 2(b) was taken for $q = 0.22q_0$, where q_0 is the momentum transfer parallel to the surface at the zone boundary. Incident beam energy was 3.0 eV and FWHM for the elastic peak was 7.4 meV. Weak peaks such as the one around 34 meV in Fig. 2(b) are stronger in the specular data [see Fig. 2(a)] and were followed continuously out from the zone center. Figure 2(c) shows a spectrum at the zone boundary. Here the beam energy was 10 eV and the FWHM was 6.0 meV. Peaks that appear around 110 meV are due to small amounts of hydrocarbon contamination. We mapped out the Brillouin zone in the $\overline{\Gamma K}$ direction. The results are plotted in Fig. 3. The resolution varied from about 6 meV to 8 meV. The uncertainty in the positions of the inelastic peaks was less than 1 meV, except for the peak closest to the elastic peak and for the 58 meV peak in the specular data, where the uncertainty was about 2 meV. All the data shown here were taken at

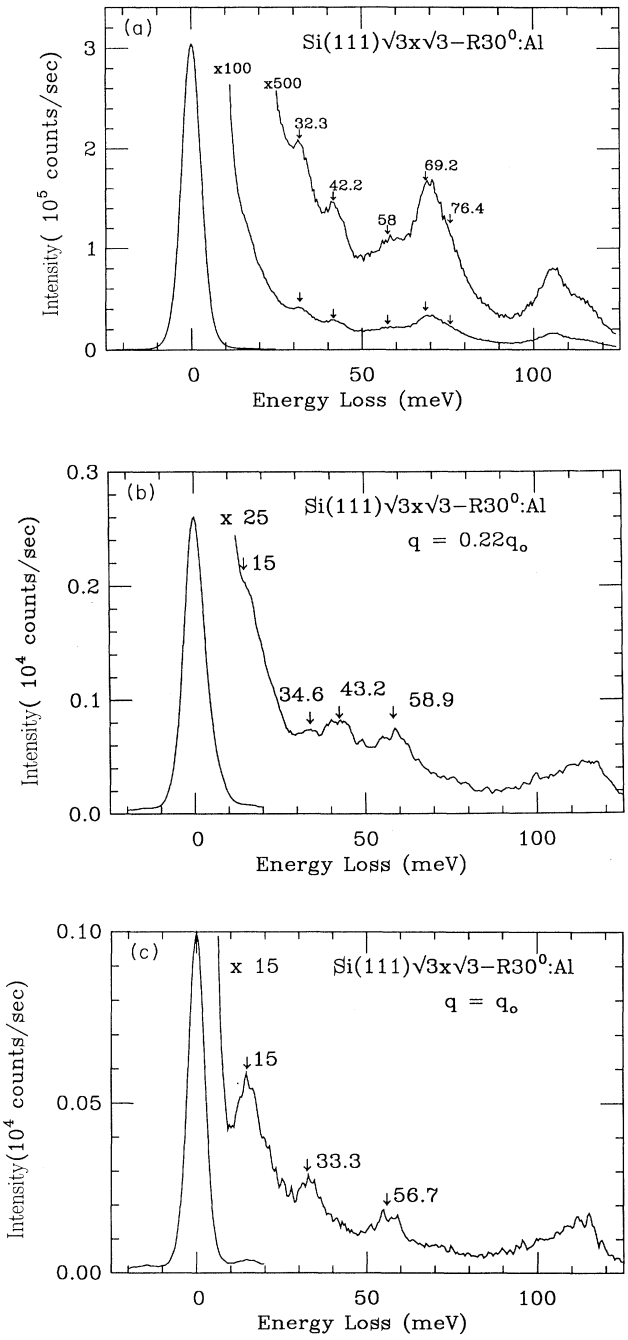

FIG. 2. Sample spectra for (a) $q = 0$, (b) $q = 0.22q_0$, (c) $q = q_0$. The arrows indicate peak positions found by optimizing the Gaussian fit. The experimental conditions are described in the text.

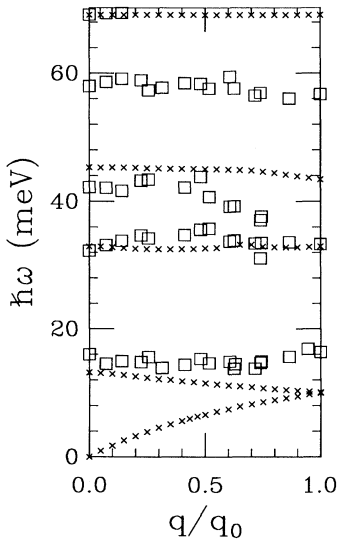

FIG. 3. Comparison of continuum model and experiment along $\overline{\Gamma K}$. The crosses mark dispersions in the model while the squares are peak positions in the experiment. Not all peaks in the calculated density of states have been plotted here (see text).

sample temperatures between 20 °C and 80 °C. A total range of 3–110 eV for the incident beam energy was used to collect the data.

III. SIMPLE MODELS OF SURFACE LATTICE DYNAMICS

This section is devoted to a description of the lattice dynamical models we use to interpret the experimental results. Neither of our two models contains a complete description of the true lattice dynamics of the adsorbate-substrate system. However, they have the merit of being parameter free, as all the force constants are uniquely determined by the results of electronic-structure calculations or by the bulk elastic constants. Both are generalizations of an earlier model introduced by Northrup.[12]

This model contained motion of only the three topmost Si layers and the Al adsorbate layer and only those motions allowed at $q = 0$, where q is the surface wave vector. The model included only seven degrees of freedom, the force constants for which were calculated in a supercell approach, using an electronic-structure calculation which had already been successful for the ground-state configuration and electronic surface states. Yet this calculation yielded very good agreement with the only observed phonon at the time of the calculation and also correctly predicted another long-wavelength phonon. Our two generalizations of this model help explain why it worked so well and also incorporate some features from the experiment.

A. Chain model for $q = 0$

In this model, we couple the force constants calculated by Northrup for the surface layers to a large number of rigid (111) planes of Si atoms modeling the substrate, allowing only motion of the planes perpendicular to the surface. By substrate, we mean those layers beneath the third Si layer, not included in the earlier calculation. The substrate here is essentially a one-dimensional chain. The equations of motion for the entire system are simply

$$\sum_{l'=1}^{N}(\omega^2\delta_{ll'} - D_{ll'})u_{l'} = 0, \tag{1}$$

where l and l' label the N coordinates and $D_{ll'}$ is the dynamical matrix for the system. For $l = 1,...,7$ the coordinates are those within the surface layers shown in Fig. 4, in which the primed and unprimed coordinates are restricted to move together. For $l > 7$, they label substrate Si(111) planes. The dynamical matrix is given in terms of the force constants for the system $K_{ll'}$ by

$$D_{ll'} = K_{ll'}/\sqrt{m_l m_{l'}}. \tag{2}$$

For a given input frequency ω we can define the Green's function for this model by

$$\sum_{l'=1}^{N}[(\omega + i0^+)^2\delta_{ll'} - D_{ll'}]G_{l'l''} = \delta_{ll''}, \tag{3}$$

from which the densities of states (DOS) of phonons can be deduced:

$$\rho_{ll'}(\omega) = -\frac{2\omega}{\pi}\mathrm{Im}[G_{ll'}(\omega)]. \tag{4}$$

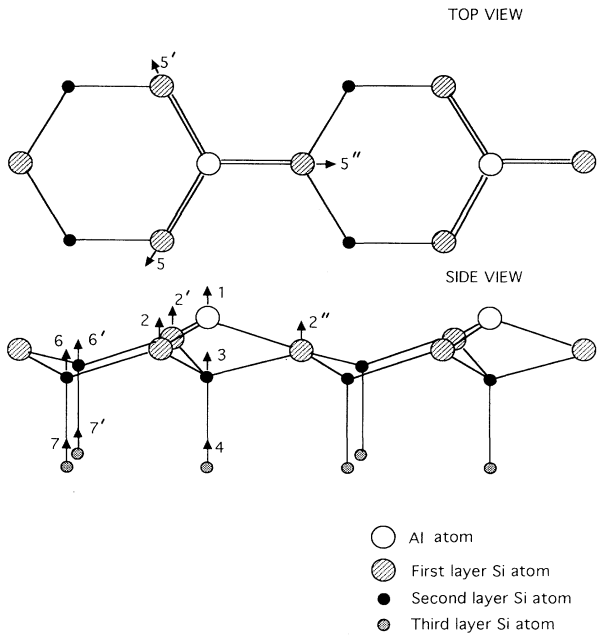

FIG. 4. Schematic of unit cell used for lattice dynamical models, where arrows indicate included coordinates. The open circle represents Al, the solid circles represent Si. The lattice repeats periodically in the parallel direction.

These satisfy the normalization condition

$$\int_0^\infty d\omega \sum_{l=1}^{N} \rho_{ll}(\omega) = N \ , \tag{5}$$

where N is the total number of degrees of freedom in the calculation. We define the surface DOS as the projection of the total DOS onto the surface coordinates

$$\rho_s(\omega) = \sum_{l=1}^{7} \rho_{ll}(\omega) \tag{6}$$

and the dipole-projected DOS as the total DOS projected onto the assumed dipole, the Al-Si stretch,

$$\rho_{\rm dip}(\omega) = \rho_{11}(\omega) + \rho_{33}(\omega) - \rho_{13}(\omega) - \rho_{31}(\omega) \tag{7}$$

using the notation displayed in Fig. 4.

The force constants for the surface layers were taken directly from Northrup's calculation. The force constants for the substrate layers were taken from a bulk calculation of interlayer (111) force constants.[16] We also took these as the coupling constants between substrate layers and surface layers. This should be a good approximation, as the lowest surface layer has an intralayer force constant close to the bulk value, and the coupling to the higher surface layers is already generally weak, because, for longitudinal motion, the interlayer force constants fall off rapidly.

The surface reconstruction poses a more difficult question. Parts of the Si surface layers can move independently of each other. For example, coordinates 4 and 7 label independent sections of a single Si(111) layer. However, the above prescription yields only force constants for rigid motions of complete planes. We remove this ambiguity by making the simplest possible assumption, namely that the restoring force between a substrate layer and a piece of a surface layer is proportional to the number of atoms (per unit surface cell) in that surface layer. We hope that this will be approximately true for the real interplanar forces. In fact, this assumption would be strictly valid if the total interplanar restoring force were due to a sum of equal forces between pairs of atoms in each plane separated by the minimum interplanar atomic distance and no force between any others, but this is unlikely to be true for Si and not necessary for our assumption to yield a good approximation. In any event, our results are insensitive to these details.

How accurate can we expect this calculation to be? We first note that $q = 0$ motions parallel to the surface have not been included. Although planar force constants are also available for bulk transverse motions, they have not been calculated for the surface layers. However, by symmetry, these are decoupled from the perpendicular motions, so their absence does not change the values of the calculated frequencies. A more serious limitation is the exclusion of bulk motions at the unreconstructed surface zone boundary point $\overline{M}$ which, due to the reconstruction, are folded into $\overline{\Gamma}$ for our surface. To include these would require a second set of interlayer force constants for the substrate. Because these are not available in the literature, we invoked the simple assumption mentioned above. The seriousness of this shortcoming is best assessed by the comparison with experiment in Sec. IV.

B. Continuum model for finite q

The above calculation works only at $q = 0$, but the experiment yields the dispersion of the phonons. To model this we need effective force constants between individual atoms and to deduce these from the force constants given by Northrup we make the same assumption as before. We assume that the restoring force produced by the motion of several atoms relative to one another is due entirely to the stretch of the bonds of smallest length, and that contributions from longer bonds are negligible. To see what this means, consider a motion in which the coordinates labeled $7, 7'$ move rigidly relative to those labeled 6 and $6'$ in Fig. 4. When these four atoms move relative to each other in this way in the original model, there is a restoring force which we attribute to the stretching of only the two shortest bonds, namely the $6-7$ and the $6'-7'$ bonds. So our assumption implies that the stretch of *any* $6-7$ bond has a force constant of $K_{67}^0/2$, where K_{67}^0 is Northrup's value, if their equilibrium separation is the shortest possible for a $6-7$ bond, and zero otherwise.

We repeat this process to deduce the force constants for all shortest bonds. In fact, the relation between these shortest distance force constants and the values in the original calculation depends only on the positions of each of the atoms in the neighboring pair within the surface plane, not on their positions in the normal direction. Note that for pairs of collective coordinates on the same set of sites, e.g., 2 and 5, the shortest distance bonds are those of individual coordinates on the same site, i.e., $(2,5)$, $(2',5')$, and $(2'',5'')$. We write the 7×7 matrix of shortest distance force constants in terms of Northrup's as

$$K_{\alpha\beta}^{\rm (SD)} = K_{\alpha\beta}^0 / S_{\alpha\beta}, \tag{8}$$

where $\alpha,\beta = 1,...,7$, $K_{\alpha\beta}^0$ is the original force constant matrix, given in Table I of Ref. 12, and where the reduction of the single-pair force constant relative to the collective-coordinate force constant is given by

$S_{\alpha\beta}$	1,3,4	2,5	6,7
1,3,4	1	3	6
2,5	3	3	6
6,7	6	6	2

Constructed in this way, the matrix $K_{\alpha\beta}^{\rm (SD)}$ contains the force constants for all the shortest distance bonds in our model.

Next we construct the force constant matrix for the entire surface. We label an individual coordinate by $(\alpha, \mathbf{L})$, where now $\alpha = 1, 2, 2', 2'', ..., 7, 7'$ labels its position within a surface unit cell and $\mathbf{L}$ labels a specific cell in the surface. Then the force constant between the $(\alpha, \mathbf{L})$th coordinate and the $(\beta, \mathbf{L}')$th coordinate is

$$K_{\alpha\beta}(\mathbf{L}-\mathbf{L}') = K_{\alpha\beta}^{\rm (SD)} \Theta(\alpha, \mathbf{L}; \beta, \mathbf{L}'), \tag{9}$$

where $\Theta(\alpha,\mathbf{L};\beta,\mathbf{L}')=0$, unless $(\alpha,\mathbf{L})$ and $(\beta,\mathbf{L}')$ are separated by the shortest distance allowed for such a pair, in which case it equals 1. Then the dynamical matrix at a given surface wave vector $\mathbf{q}$ is[22]

$$D_{\alpha\beta}(\mathbf{q})=\sum_{\mathbf{L}}\frac{K_{\alpha\beta}(\mathbf{L})}{\sqrt{m_\alpha m_\beta}}e^{i\mathbf{q}\cdot\mathbf{L}}, \tag{10}$$

where m_1 is the mass of Al and m_α for all other values of α is the mass of Si. Here the sum over $\mathbf{L}$ includes all surface unit cells, but in our case, only the $L=0$ and nearest-neighbor cells have nonzero contributions. Finally, to find the frequencies and eigenvectors, one solves the 13×13 eigenvalue equation

$$\sum_{\beta=1}^{13}[\omega^2\delta_{\alpha\beta}-D_{\alpha\beta}(\mathbf{q})]u_\beta(\mathbf{q})=0. \tag{11}$$

This yields 13 modes for each value of q, which we could compare with the experimentally observed modes.

However, the model as stated above would still include only the first few surface layers and therefore be missing any long-wavelength acoustic modes. To overcome this difficulty, we couple the surface layers to a continuum model for the Si substrate. We follow the method used by Morse and Mele[6] to analyze the Rayleigh wave on As:Si(111). The restoring forces which previously coupled the surface layers to an immobile background now couple them to the surface of an elastic Si continuum. The equations of motion and their solution are described in some detail by Morse and Mele, and here we only state the solution, generalized to allow several surface degrees of freedom. We define the Green's function for the substrate elastic continuum as obeying stress-free boundary conditions and the inhomogeneous equation

$$\sum_{j=1}^{3}\left(\omega^2\delta_{ij}+\frac{1}{\rho}\sum_{km}C^{ikjm}\partial_k\partial_m\right)g_{ij}^{(\mathrm{subs})}(\omega;\mathbf{R}-\mathbf{R}',z,z')=\delta_{ij}\delta^{(3)}(\mathbf{r}-\mathbf{r}'), \tag{12}$$

where i,j represent Cartesian coordinates, ρ is the density of the medium, $\{C^{ikjm}\}$ are the elastic constants of the medium, and $g_{ij}^{(\mathrm{subs})}(\omega;\mathbf{R}-\mathbf{R}',z,z')$ is the three-dimensional Green's function, evaluated at frequency ω and positions $\mathbf{r}=(\mathbf{R},z)$ and $\mathbf{r}'=(\mathbf{R}',z')$. We next project this onto the coordinates of the surface layers by defining

$$G_{\alpha\beta}^{(\mathrm{subs})}(\omega,\mathbf{q})=e^{i\mathbf{q}\cdot(\mathbf{R}_\alpha-\mathbf{R}_\beta)}\frac{\sqrt{m_\alpha m_\beta}}{\rho A}\times\hat{\mathbf{e}}_\alpha\cdot\mathbf{g}^{(\mathrm{subs})}(\omega,\mathbf{q})\cdot\hat{\mathbf{e}}_\beta, \tag{13}$$

where $\mathbf{g}^{(\mathrm{subs})}(\omega,\mathbf{q})$ is the three-dimensional Green's function, Fourier transformed in the parallel direction and evaluated at the surface, i.e.,

$$g_{ij}^{(\mathrm{subs})}(\omega,\mathbf{q})=\int d^2R\,e^{i\mathbf{q}\cdot\mathbf{R}}g_{ij}^{(\mathrm{subs})}(\omega;\mathbf{R},z=0,z'=0). \tag{14}$$

In Eq. (13) α and β label the allowed degrees of freedom of the surface atoms, $\mathbf{e}_\alpha$ are their directions, $\mathbf{R}_\alpha$ are their positions within the surface plane, m_α are their masses, and A is the area of a surface unit cell. This projected Green's function is then coupled to the dynamical matrix of Eq. (10) to yield a T matrix which, in matrix notation, is just

$$T(\omega,\mathbf{q})=[1-D(\mathbf{q})G^{(\mathrm{subs})}(\omega,\mathbf{q})]^{-1}D(\mathbf{q}). \tag{15}$$

This T matrix is an effective dynamical matrix for the coupled system, as the equations of motion are

$$\sum_{\beta=1}^{13}[\omega^2\delta_{\alpha\beta}-T_{\alpha\beta}(\omega,\mathbf{q})]u_\beta=0, \tag{16}$$

analogous to Eq. (9) of Ref. 6. The Green's function for the coupled system is then

$$G(\omega,\mathbf{q})=[(\omega+i0^+)^2-T(\omega,\mathbf{q})]^{-1}, \tag{17}$$

from which the DOS may be easily calculated:

$$\rho_{\alpha\beta}(\omega,\mathbf{q})=-\frac{2\omega}{\pi}\mathrm{Im}[G(\omega;\mathbf{q})_{\alpha\beta}] \tag{18}$$

analogous to Eq. (4).

The physics behind this coupling can be seen in the definition of the T matrix, Eq. (15). We can imagine a rigid substrate as one having infinite mass density, thereby making $G^{(\mathrm{subs})}=0$, so that the T matrix is just the dynamical matrix of the original problem. On the other hand, for small ω and q, $G_{\alpha\beta}^{(\mathrm{subs})}(\omega,\mathbf{q})$ becomes very large, so that the T matrix is just the inverse of the projected Green's function of the continuum, and the dynamics of the substrate dominate. In practice, we find the two sources of dynamical response contributing differently in different regimes.

The calculation of densities of states for this model is not much more difficult than for a rigid substrate. We approximate the Si substrate Green's function by that of a semi-infinite isotropic medium, with longitudinal and transverse velocities set equal to their Si values along the $\overline{\Gamma K}$. In that case, analytic expressions are known[23] for $g_{ij}^{(\mathrm{subs})}(\omega;\mathbf{R}-\mathbf{R}',z,z')$. For each pair of values (ω,q), one then only needs to multiply and invert several 13×13 matrices.

The results of such a calculation are semiquantitative at best. An exact calculation would include the correct interatomic forces and a discrete model of the substrate Si. However, overall trends and rough numbers should be correct, yielding some insight into the physics involved.

IV. INTERPRETATION OF EXPERIMENTAL RESULTS

Figure 5 is a picture of DOS calculated in the chain model. The solid curve is the surface-projected DOS, the dotted curve is the dipole-projected DOS, and the arrows indicate the positions of the three observed vibrations we can expect to see in this model (see below). In practice, we replace 0^+ in Eq. (4) by a small finite value

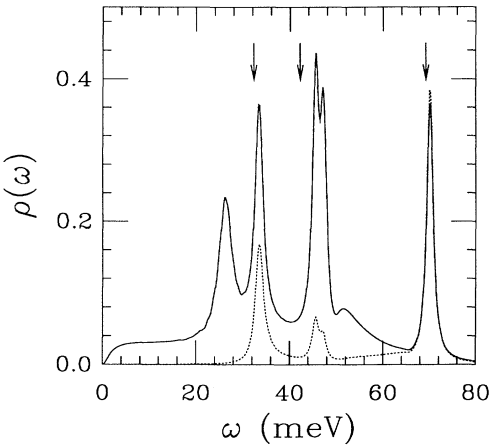

FIG. 5. Densities of states (in arbitrary units) for the chain model of $q = 0$ perpendicular vibrations. The solid line is the surface-projected density, the dotted line is the dipole-projected density, and the arrows indicate the positions of experimental peaks of modes which can be expected to appear in the chain model.

(0.8 meV) in all our calculations of DOS to broaden very sharp resonances for plotting and to smooth over any roughness due to using finite length chains. Note that we do not distinguish here between true surface modes and strong resonances, as we have not included all contributions from bulk modes in this model. The figure shows that, while there are several modes at the surface, only three have a strong dipole projection: 69 meV, 45 meV, and 33 meV. The first and last of these are discussed by Northrup and are essentially unchanged by the addition of the substrate layers. The displacements of the surface atoms in the 45-meV mode are shown in Fig. 6. This mode is predominantly a breathing mode of the cluster comprising the Al, the three nearest Si atoms in the next layer, and the two Si atoms directly beneath. There is also a small contribution from another mode at 47 meV, which is essentially a vertical vibration of the top Al and Si layers relative to the bottom two Si layers. The frequencies of these modes are sufficiently close to make them experimentally indistinguishable, and besides, neither exactly correspond to the observed mode energy of 42 meV. This small discrepancy may be attributed to simplifying assumptions of the chain model (see Sec. III A). The good agreement between peaks in the dipole-projected DOS of the Al:Si stretch and the $q = 0$ peaks of the experiment is consistent with the strongest dipole lying along this bond.

This calculation improves upon the earlier calculation[12] in several ways. Most importantly, we see that most of the modes found in that calculation are insensitive to the details of the substrate, because the cluster at the surface is so tightly bound together. This explains the success of the few surface layer model for the modes observed. Second, the original calculation produces a spurious mode at 15 meV, in which the surface layers move rigidly relative to the fixed substrate. This artifact does not appear in the chain model, which includes modes with frequencies ranging continuously down to zero. Finally, another mode appears in the original calculation at 41 meV, a mode which would also be a candidate for the peak in the experiment at 42 meV. The chain model shows that, when coupling to the substrate layers is included, the dipole-projected DOS for this mode becomes very weak, and so it does not appear in this more realistic calculation.

Next we consider the dispersion of the surface modes. In Fig. 3 we plot both the experimental (squares) and theoretical (solid lines) dispersions of modes along $\overline{\Gamma K}$. The calculation is that described in Sec. III B. We have included in the theory plot only those peaks which correspond with experimentally observed modes. Other peaks appearing in the surface-projected DOS have not been shown as, without experimental verification, and in the absence of a more sophisticated calculation, there is no way to determine if they are artifacts of the model.

As the figure indicates, the three modes at 33 meV, 45 meV, and 69 meV disperse very little across the Brillouin zone, in qualitative agreement with the experiment. Furthermore, the eigenvectors are almost unchanged out to the zone boundary. Note that as many of the coordinates included in the model represent motions of atoms perpendicular to the surface, most of the modes are transverse modes, i.e., dominated by transverse motions. This is true for all the modes plotted in Fig. 3.

The dipole-projected DOS of this model at $q = 0$ is very similar to that of the chain model of Fig. 5. However, for finite q, this projection is not so useful, dipole scattering no longer dominates. We have studied the

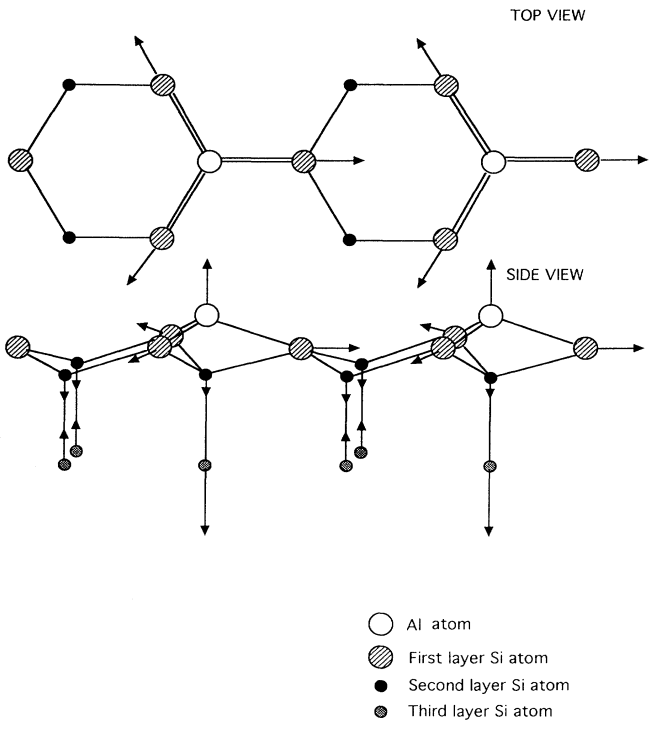

FIG. 6. Motions of atoms in the 45-meV mode at $q = 0$. Lengths of arrows represent sizes of displacements.

intensities of the experimental peaks as a function of angle away from specular in an attempt to determine which modes are seen by impact scattering and which are dipole active.[17] Only the intensity of the 69-meV peak follows the intensity of the elastic peak as q grows, so much so that this peak was no longer visible beyond about a quarter of the way through the zone. This suggests that this mode is strongly dipole active.[17] All others showed evidence of impact scattering, i.e., the peaks remained strong even out to the zone boundary.

Now we discuss how the Rayleigh mode was plotted in Fig. 3. We calculated the optical branch of this mode, due to the folding back of the unreconstructed surface Brillouin zone, simply by extending the calculation to values of **q** into a neighboring zone, from $\overline{K}$ to $\overline{\Gamma}$ in that zone. As the elastic continuum contains no information about the lattice structure, and in particular about the surface reconstruction, the Rayleigh mode continues to disperse beyond the boundary of the first Brilloin zone. This dispersion was then reflected back into the original zone and plotted on Fig. 3. Note that in general the theory predicts a dispersion somewhat lower than was found in the experiment. This can be attributed to two effects: the lack of a zone-boundary gap, which ought to be present due to the reconstruction, and the tendency of the continuum model to underestimate the Rayleigh wave frequency.[23] Note that the experimental results are close to those for the Si(111)-(1 × 1):H surface, both at $\overline{\Gamma}$ [compare with $\overline{M}$ on the (1 × 1) surface] and at $\overline{K}$ [compare with the mipoint of $\overline{\Gamma M}$ on the (1 × 1) surface].

So far we have avoided discussing the mode observed at 60 meV in the experiment. Why does it not appear in the theory, especially in the chain model at $q = 0$? We suggest this may be a Lucas mode which does not appear in the chain model either because it has been folded back from the unreconstructed zone boundary to $\overline{\Gamma}$ or because it is polarized parallel to the surface. Modes at similar energies have been found in both experiments[18,19] and calculations[4,19,24] on both Si(111) (2 × 1) and Si(111)-(1 × 1):H. The detailed nature of this mode must await a fuller theoretical description of the lattice dynamics than that presented here.

We conclude this section with the results of further calculations based on this model. We have calculated the surface phonons along all high symmetry directions in the Brillouin zone and found results qualitatively similar to those discussed above. Such calculations can easily be reproduced by following the prescription given in Sec. III. In Fig. 7 we have repeated the calculation without changing any force constants, but by replacing the Al mass by that of In. The modes are qualitatively similar to those in Al, with small changes in their frequencies, except for that at about 15 meV. This mode *is* the folded-back Rayleigh mode for this surface, appearing here in the chain model. In this case, the heavy adsorbate imposes the characteristic displacement pattern of a folded-back eigenvector on the neighboring Si atoms, even though the substrate layers are restricted to rigid motions. The true mode has the folded-back motion allowed in the substrate layers and so can be expected to have a slightly different frequency.

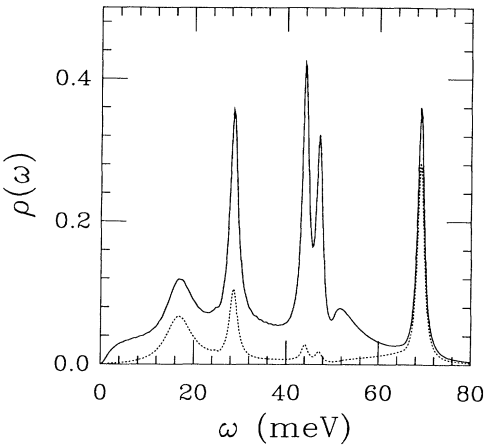

FIG. 7. Density of states calculated in the chain model for In/Si(111) along $q = 0$, assuming the same force constants as Al.

V. CONCLUSIONS

An angle-resolved HREELS study of the Si(111)-$(\sqrt{3} \times \sqrt{3})R30°$:Al surface has been performed and several surface phonons observed. These have been interpreted using two very simple models for the lattice dynamics, which together reproduce all the modes seen in the experiment, with the exception of an almost dispersionless mode at 58 meV. Both of these models include the bulk lattice dynamics in some form. Their chief defect lies in their incompleteness, when compared with more sophisticated lattice dynamical models in state of the art calculations.[3] However, because the force constants have been deduced from an electronic-structure calculation, these models have no adjustable parameters. Thus comparison with experiment provides an unambiguous test of their validity. This is to be contrasted with many larger calculations, based on phenomenological models for the dynamics, in which the force constants are fit to the bulk dispersion curves and may be further adjusted at the surface. The usefulness of such a procedure can be undermined by the nonuniqueness of such a fit.[25] Furthermore, our model is easy to program (the calculations may be performed on a personal computer) and conceptually straightforward, so that the underlying physics can be easily understood. Such a simple approach may prove very useful to experimentalists working on other surfaces, especially when deciding what might be interesting to look at.

While the agreement with experiment is satisfying, there is much work yet to be done. This agreement provides strong evidence that the force constants are correct and could be coupled to a full calculation employing bulk interatomic Si force constants to get the full dispersion curves. The results of such a calculation should not differ markedly from those given here, while a peak intensity analysis could be performed using multiple-scattering theory.[26] These should provide further evidence for the validity of the electronic-structure calculation. Also, He scattering experiments could be done[27] to plot out the full Rayleigh wave dispersion curve

to further bolster our understanding of this system and to justify a more sophisticated calculation.

ACKNOWLEDGMENTS

We are grateful to Bob Phelps, Kieran Mullen, and Bill Schaich for useful discussions, and to John Northrup for enlightening conversations about his lattice dynamical model. This work was supported by the U.S. Department of Energy through Grant No. DE-FG02-84ER45147 (P.A., G.G., and L.K.), and by the National Science Foundation under Grant No. DMR-89-03851 (K.B.).

* Present address: Department of Physics, Clarion University of Pennsylvania, Clarion, PA 16214.
† Author to whom correspondence should be addressed.

[1] For a recent example, see Karl D. Brommer, M. Needels, B. E. Larson, and J. D. Joannopoulos, Phys. Rev. Lett. **68**, 1355 (1992).
[2] For a review of surface lattice dynamical calculations, see, for example, *Surface Phonons*, edited by W. Kress and F. W. de Wette (Springer-Verlag, Berlin, 1991).
[3] D. C. Allan and E. J. Mele, Phys. Rev. B **31**, 5565 (1985).
[4] O. L. Alerhand, D. C. Allan, and E. J. Mele, Phys. Rev. Lett. **55**, 2700 (1885).
[5] D. C. Allan and E. J. Mele, Phys. Rev. Lett. **53**, 826 (1984).
[6] D. C. Morse and E. J. Mele, Phys. Rev. B **40**, 3465 (1989).
[7] E. J. Mele, D. C. Allan, O. L. Alerhand, and D. P. DiVincenzo, J. Vac. Sci. Technol. B **3**, 1068 (1985).
[8] H. Huang, S. Y. Tong, W. S. Yang, H. D. Shih, and F. Jona, Phys. Rev. B **42**, 7483 (1990).
[9] J. M. Nicholls, B. Reichl, and J. E. Northrup, Phys. Rev. B **35**, 4157 (1987).
[10] J. E. Northrup, Phys. Rev. Lett. **53**, 683 (1984).
[11] Northrup's result for the ground-state configuration has been further verified by a first-principles molecular-dynamics simulation; see H. Tsuge, M. Arai, and T. Fujiwara, Jpn. J. Appl. Phys. **30**, L1583 (1991).
[12] J. E. Northrup, Phys. Rev. B **39**, 1434 (1989).
[13] M. K. Kelly, G. Margaritondo, J. Anderson, D. J. Frankel, and G. J. Lapeyre, J. Vac. Sci. Technol. A **4**, 1396 (1986).
[14] M. K. Kelly, G. Margaritondo, J. Anderson, D. J. Frankel, and G. J. Lapeyre, J. Vac. Sci. Technol. A **4**, 1481 (1985).
[15] G. S. Glander, P. Akavoor, and L. L. Kesmodel, Phys. Rev. B **44**, 5893 (1991).
[16] A. Fleszar and R. Resta, Phys. Rev. B **34**, 7140 (1986).
[17] H. Ibach and D. L. Mills, *Electron Energy Loss Spectroscopy and Surface Vibrations* (Academic Press, New York, 1982).
[18] H. Ibach, Phys. Rev. Lett. **27**, 253 (1971).
[19] U. Harten *et al.*, Phys. Rev. B **38**, 3305 (1988).
[20] D. Roy and J.D. Carette, in *Electron Spectroscopy for Surface Analysis*, edited by H. Ibach (Springer, Berlin, 1977); Can. J. Phys. **49**, 2138 (1971); D. Roy, A. Delage, and J.D. Carette, J. Phys. E **8**, 109 (1975).
[21] L.L. Kesmodel, J. Vac. Sci. Technol. A **1**, 1456 (1983).
[22] See N. W. Ashcroft and N. D. Mermin, *Solid State Physics* (Holt, Rinehart, Wilson, Philadelphia, 1976).
[23] A. A. Maradudin and D. L. Mills, Ann. Phys. (N.Y.) **100**, 262 (1976).
[24] L. Miglio *et al.*, Phys. Rev. Lett. **62**, 3070 (1989).
[25] F. W. de Wette, in *Surface Phonons*, edited by W. Kress and F. W. de Wette (Springer-Verlag, Berlin, 1991), p. 67.
[26] D. L. Mills, S. Y. Tong, and J. E. Black, in *Surface Phonons*, edited by W. Kress and F. W. de Wette (Ref. 25), p. 193.
[27] R. B. Doak and D. B. Nguyen, Phys. Rev. B **41**, 3578 (1990).